Inorganic Chemistry

Article

pubs.acs.org/IC

Bispidine Dioxotetraaza Macrocycles: A New Class of Bispidines for ^{64}Cu PET Imaging

Peter Comba,*[,†] Manja Kubeil,[‡] Jens Pietzsch,[‡,§] Henning Rudolf,[†] Holger Stephan,*[,‡] and Kristof Zarschler[‡]

[†]Anorganisch-Chemisches Institut, Universität Heidelberg, INF 270, D-69120 Heidelberg, Germany

[‡]Institute of Radiopharmaceutical Cancer Research, Helmholtz-Zentrum Dresden-Rossendorf, D-01314 Dresden, Germany

[§]Fachrichtung Chemie und Lebensmittelchemie, Technische Universität Dresden, D-01062 Dresden, Germany

Supporting Information

ABSTRACT: The three new dioxo-tetraazamacrocyclic ligands with a fused, very rigid bispidine (3,7-diazabicyclo[3.3.1]nonane) group connecting the two tertiary amine donors, and ethyl, propyl, or benzene groups connecting the two amide donors are highly preorganized and lead to very stable, uncharged Cu^{II} complexes. Solution spectroscopy and solid state structures indicate that these are square pyramidal with a solvent molecule occupying the apical position. Cyclic voltammetry defines a reversible $Cu^{III/II}$ couple and a strongly negative irreversible $Cu^{II/I}$ couple (ca. −2 V vs Fc/Fc^{+}), indicating that the Cu^{II} complexes are very stable in solution. This is supported by superoxide dismutase (SOD) and human serum challenge experiments as well as the biodistribution, which all show that the benzene-based ligand has the highest *in vitro* and *in vivo* stability and that this was expected on the basis of the macrocycle ring size and shape and the highest degree of preorganization. This ligand is easy to functionalize for a possible coupling to biological vector molecules and/or fluorescence markers for PET (positron emission tomography) and multimodal imaging (i.e., PET and optical imaging).

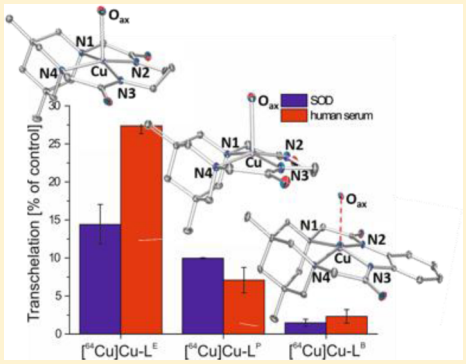

INTRODUCTION

There is increasing interest in the development of applications of radiotracers for cancer diagnosis. An important method is positron emission tomography (PET), where a radioactive positron emitting isotope is linked to a biological vector such as a protein, peptide, or aptamer that specifically accumulates in cancer cells. With positron emitters, for example ^{64}Cu ions, an important focus is on the design of bifunctional chelators (BFCs) that coordinate the β^{+} emitting metal ion with high stability and offer functional groups for conjugation to biological vector molecules. Because of its suitable half-lifetime of 12.7 h and its decay scheme (β^{+}, 19%; β^{-}, 40%; and electron capture 40%), ^{64}Cu is an ideal positron emitter for PET imaging, and the "matched-pair" ^{64}Cu/^{67}Cu offers possible applications in diagnosis and therapy.[1−5] There is a range of well-known ligand systems for stable and well-defined Cu^{II} complexes, and derivatives of these ligands have been used as BFCs for PET imaging. Examples are ATSM (diacetyl-bis(*N*4-methylthiosemicarbazone),[6,7] derivatives of aza-macrocycle ligand systems, including TETA and DOTA,[8−13] derived from the 14- and 12-membered cyclam- and cyclen-type aza-macrocycles, and hexamine cage ligands.[14−16] An advantage of these systems is the high thermodynamic stability (macrocyclic effect[17,18]) and facile methods for the attachment of functionalities such as carboxylates, where a biofunctionalization can be performed. However, some of the corresponding Cu^{II} complexes have been shown to have too low *in vivo* stabilities, for example, some are decomposed *in vivo* by superoxide dismutase and ceruloplasmin.[19−21] Also, the synthesis of polyaza macrocycles and the corresponding bioconjugates may be tedious (multiple step syntheses),[22−25] and complex formation may be slower than that required for *in vivo* PET imaging.[4]

Dioxotetraaza macrocyclic ligands have attracted interest for a number of reasons: due to the macrocycle effect and the stabilization by two deprotonated amide nitrogen donors, they are known to form highly stable and uncharged Cu^{II} complexes; and due to the deprotonated amide donors, these ligands are also known to stabilize Cu^{III}.[26,27] In the context of PET imaging, it is specifically the high stability of the uncharged Cu^{II} complexes that has attracted our attention.[28−30] Another ligand backbone known for its suitability as a BFC for ^{64}Cu-based PET imaging is the highly preorganized bispidine platform with its rigid adamantane-derived 3,7-diazabicyclo[3.3.1]nonane backbone.[31−35] This type of ligand, first discovered by Mannich and Mohs,[36] offers a widely variable donor set which allows the fine-tuning of the electronic properties of the resulting complexes.[32,34] There is a wide range of applications of bispidine transition metal chemistry,[32,37,38] but there are only few reports

Received: February 28, 2014
Published: June 6, 2014

   dx.doi.org/10.1021/ic500476u | *Inorg. Chem.* 2014, 53, 6698−6707

Chart 1. Ligands Discussed

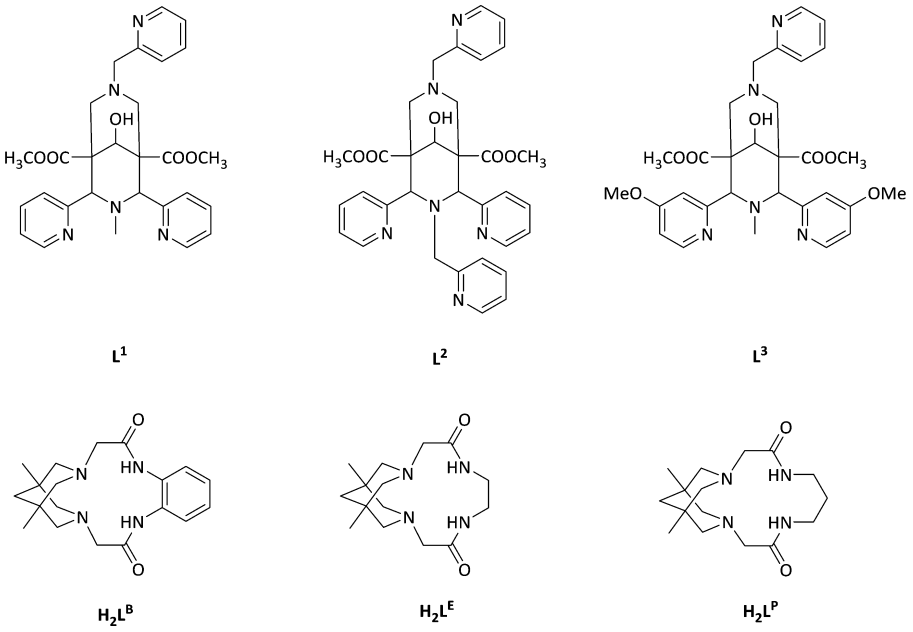

Scheme 1. Synthesis of the Macrocyclic Ligands H_2L^B, H_2L^E, and H_2L^P

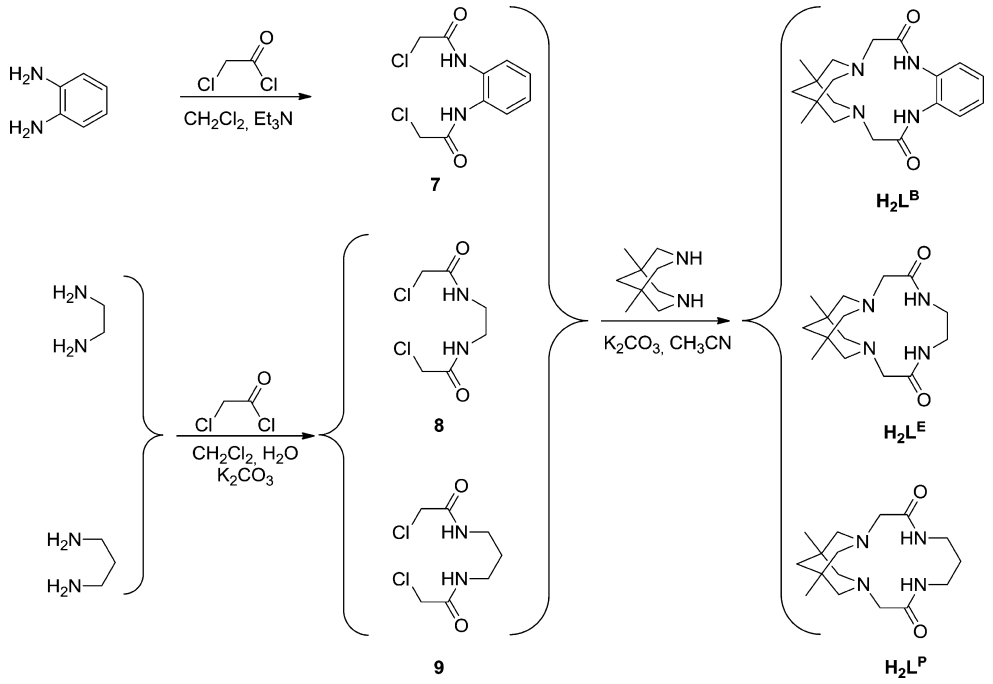

on macrocyclic bispidines[39,40] and uncharged Cu^{II} complexes of bispidine-based ligands.[41]

Here, we combine the two motifs of the dioxotetraaza macrocycles with the rigidity of the bispidine backbone and report the synthesis of three derivatives of a new type of ligand with varying ring size and preorganization, L^B, L^E, and L^P (see Chart 1), together with their Cu^{II} complexes.

RESULTS AND DISCUSSION

Synthesis. The three macrocycles H_2L^B, H_2L^E, and H_2L^P were synthesized by cyclization of 5,7-dimethyl-1,3-diazabicyclononane[42] with the bis(α-chloroacetamide) of the corresponding diamine (Scheme 1). The use of bis(α-chloroacetamides)[43] has found broad application in the synthesis of dioxotetraaza macrocycles.[28] 1,2-Diaminoethane, 1,3-diaminopropane, and *o*-phenylendiamine were condensed with chloroacetyl chloride to yield the bis(α-chloroacetamide) building blocks; [1 + 1] condensation with 5,7-dimethyl-1,3-diazabicyclononane, the bispidine building block, resulted in acceptable yields of the macrocycles H_2L^B (65%), H_2L^E (34%), and H_2L^P (74%). The Cu^{II} complexes of the three macrocycles were prepared by reaction of the ligand with an equimolar amount of copper(II) acetate hydrate in methanol overnight; suitable crystals for X-ray diffraction were obtained by ether diffusion or evaporation of the methanolic complex solution at ambient temperature.

dx.doi.org/10.1021/ic500476u | Inorg. Chem. 2014, 53, 6698−6707

Crystal Structures. The molecular structures of the ligands are shown in Figure 1. In each of the structures, one of the

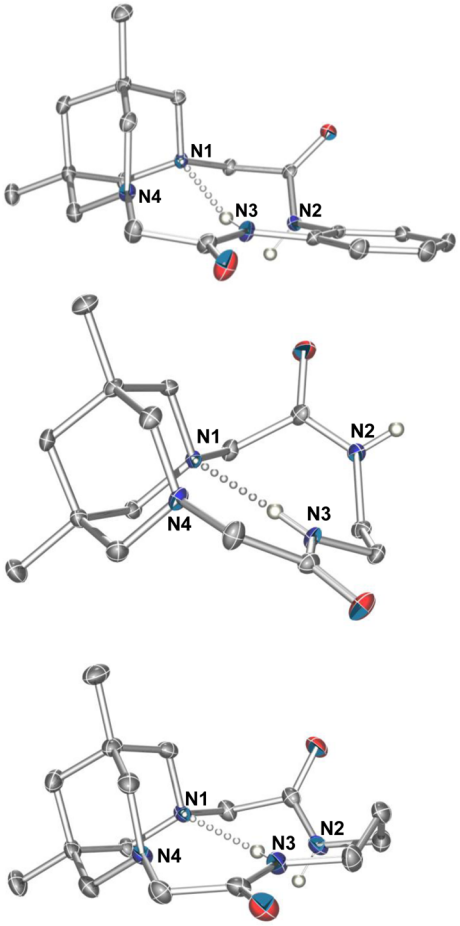

Figure 1. ORTEP (POV-ray) plots of the ligands H_2L^B, H_2L^E, and H_2L^P; hydrogen atoms have been omitted for clarity, and ellipsoids are shown at 50% probability.

amide protons is pointing toward the opposite tertiary amine, stabilized by hydrogen bonding with N−H···N distances of 2.767(13) Å (H_2L^B), 2.183(13) Å (H_2L^E), and 2.908(8) Å (H_2L^P) [hydrogen atoms are located at calculated positions, and the corresponding N···N distances are 3.6360(19) Å (H_2L^B), 3.067(2)Å (H_2L^E), and 3.7626(12) Å (H_2L^P)]. The other amide proton is located proximal to the mean plane defined by the four nitrogen donors of the macrocycle (N_4 plane). The hole size of the macrocyclic ligands[44] increases in the order 1.875 Å (H_2L^B) < 1.962 Å (H_2L^E) < 2.042 Å (H_2L^P), i.e., in terms of cavity size, H_2L^P appears to be the most suitable ligand for Cu^{II}. Affected by the rigidity of both the bispidine backbone and the benzyl ring as well as the planarity of the amide groups, H_2L^B shows the highest degree of rigidity and preorganization.[45−47] Both H_2L^P and H_2L^B are largely planar macrocyclic ligands, and H_2L^E, due to the puckered ethylene bridge, shows a slightly more distorted N_4 arrangement.

Plots of the experimental molecular structures of the Cu^{II} complexes of H_2L^B, H_2L^E, and H_2L^P appear in Figure 2, and selected geometric parameters are listed in Table 1. The two amides are deprotonated in all three complexes, leading to neutral molecules. [$Cu(L^B)(O)$] has a slightly distorted square pyramidal coordination geometry with the copper center displaced by 0.38 Å from the N_4 plane; this is not unexpected

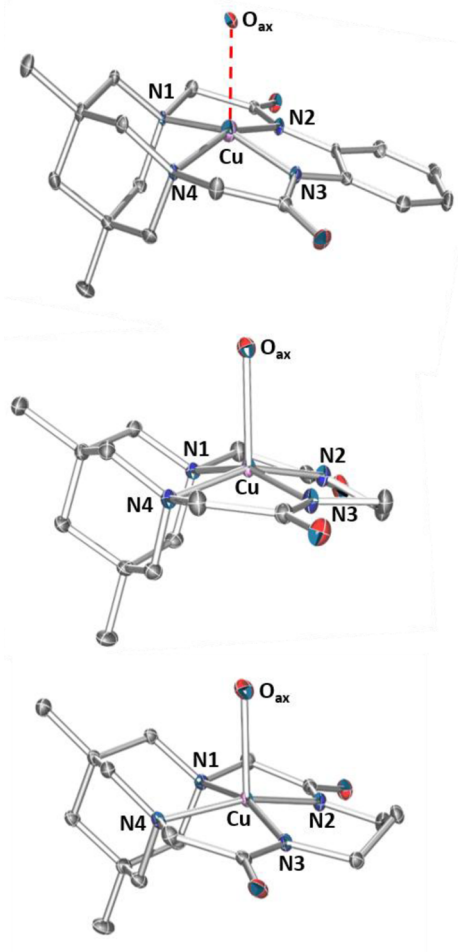

Figure 2. ORTEP (POV-ray) plots of the complexes [$Cu(L^B)(O)$], [$Cu(L^E)(OH_2)$], and [$Cu(L^P)(OH_2)$]; hydrogen atoms have been omitted for clarity, and ellipsoids are shown at 50% probability.

Table 1. Selected Bond Distances and Angles of [$Cu(L^B)(O)$], [$Cu(L^E)(OH_2)$], and [$Cu(L^P)(OH_2)$]

distance (esd) [Å]	[$Cu(L^B)(O)$]	[$Cu(L^E)(OH_2)$]	[$Cu(L^P)(OH_2)$]
Cu−N(1)	1.972(3)	1.9935(8)	2.0193(17)
Cu−N(2)	1.898(2)	1.9006(8)	1.9356(16)
Cu−N(3)	1.898(3)	1.8890(9)	1.9332(14)
Cu−N(4)	1.984(3)	1.9841(8)	2.0352(17)
Cu−O_{axial}	2.300(2)	2.3239(8)	2.3942(16)
N(1)···N(4)	2.862(4)	2.8783(11)	2.819(2)
Cu···N_4 (out-of-plane)	0.38(13)	0.37(4)	0.27(10)
angle (esd) [deg]	[$Cu(L^B)(O)$]	[$Cu(L^E)(OH_2)$]	[$Cu(L^P)(OH_2)$]
N(1)−Cu−N(2)	87.40(12)	87.05(3)	84.84(7)
N(2)−Cu−N(3)	85.19(12)	85.82(4)	96.94(8)
N(3)−Cu−N(4)	87.41(12)	86.23(4)	85.45(8)
N(4)−Cu−N(1)	92.71(12)	92.71(3)	88.08(7)

since a 13-membered macrocycle is known to be slightly too small for Cu^{II}.[48] The analysis of the unit cell reveals that the coordination of the copper center is completed by an axial amide oxygen of a neighboring molecule at 2.300 Å (see Supporting Information). A square pyramidal coordination geometry is also in agreement with the (solution) spectroscopic data (see below; for this reason, the L^B-derived complex is described as [$Cu(L^B)(O)$] in the crystal structure and generally as [$Cu(L^B)(solv)$] since we assume that, in solution, a solvent

dx.doi.org/10.1021/ic500476u | Inorg. Chem. 2014, 53, 6698−6707

molecule (e.g., OH_2) coordinates in an apical position, leading to a square pyramidal structure as in the crystal and with the other ligands).

The molecular structure of the other complex with a 13-membered macrocycle, $[Cu(L^E)(OH_2)]$, is similar to that of $[Cu(L^B)(O)]$. The distances of the donor atoms to the copper center are on average 0.004 Å longer, and this is attributed to the more flexible and approximately 0.118 Å longer ethyl bridge (observed N···N distance in the experimental structures). The emerging slightly larger cavity also leads to a decrease of the displacement of the copper center from the N_4 plane by 0.013 Å. In this structure, a water molecule is coordinated as an axial ligand, completing the square pyramidal coordination sphere.

H_2L^P is the only one of the three ligands with a 14-membered macrocyclic ring, known to be complementary for Cu^{II}. Because of the larger cavity, the copper center is less displaced from the center of the macrocyclic ring by 0.1 Å compared to $[Cu(L^B)(O)]$ and $[Cu(L^E)(OH_2)]$. The mean Cu−N distances are 0.044 Å (0.038 Å) longer than these in $[Cu(L^B)(O)]$ ($[Cu(L^E)(OH_2)]$), but the distance of the two bispidine nitrogens N(1) and N(4) decreases by 0.053 Å (0.059 Å). This emerges from the larger propylene bridge in $[Cu(L^P)(OH_2)]$, leading to a slightly expanded N(2)−Cu−N(3) angle. Similar to $[Cu(L^E)(OH_2)]$, $[Cu(L^P)(OH_2)]$ has a coordinated water molecule in the apical position, resulting in a square pyramidal coordination geometry.

The structural reorganization parameter $\Sigma_{n=1}^{6}|\Delta d_n|$ offers the opportunity to quantify the degree of preorganization of a ligand. The structural reorganization is the sum of deviation of donor atom···donor atom distances upon coordination of the ligand to a metal ion.[45] The comparatively small values of $\Sigma_{n=1}^{6}|\Delta d_n|$ indicate a high degree of preorganization,[45] and the calculated structural reorganization parameters for the ligands H_2L^B, H_2L^E, and H_2L^P validate the assumption that the degree of preorganization decreases in the row H_2L^B (0.44) > H_2L^P (0.91) > H_2L^E (1.21).

Electronic Properties. The UV−vis spectra were recorded in methanolic solution, and the absorption maxima and extinction coefficients are presented in Table 2 (see Supporting Information for the spectra). Compared to the 13-membered ring systems of $[Cu(L^B)(solv)]$ and $[Cu(L^E)(OH_2)]$, the dd transitions (asymmetric absorption band involving the $t_{2g} \rightarrow d_{x2-y2}$ transitions) of $[Cu(L^P)(OH_2)]$ with a 14-membered macrocyclic ligand are shifted by close to 2,000 cm^{-1} to lower energy. This is due to the expected decrease of the ligand field due to slightly longer bonds. This indicates that the solution structures are similar to those observed in the crystals (see above), and this also agrees with the frozen solution EPR parameters discussed below. Interestingly, the electronic properties of the dioxotetraaza macrocyclic ligand Cu^{II} complexes not supported by bispidine platforms (electronic spectra also given in Table 2) indicate that the optimum ring size in that case is 14, and this is similar to what is observed for tetraaza macrocycles.[48] The increased rigidity of the bispidine-type systems discussed here leads to a modification of the structural and thermodynamic properties, and this also emerges from the structural analysis above.

Table 2. Maxima in Absorption and Extinction Coefficients of the Cu^{II} Complexes of H_2L^B, H_2L^E, and H_2L^P (Measured in MeOH) and Literature-Known Dioxo-Tetraaza Macrocyclic Ligands

	λ [nm]	ν [cm^{-1}]	ε [$M^{-1}\cdot cm^{-1}$]
$[Cu(L^B)(solv)]$	483	20,700	149
$[Cu(L^E)(OH_2)]$	476	21,010	117
$[Cu(L^P)(OH_2)]$	524	19,080	189
$[Cu(dioxo(12)aneN_4)]$	620	16,130	150[26]
$[Cu(dioxo(13)aneN_4)]$	520	19,230	100[26]
$[Cu(dioxo(14)aneN_4)]$	505	19,800	100[26]
$[Cu(dioxo(15)aneN_4)]$	520	19,230	100[26]

The experimental EPR spectra were recorded in frozen solution in MeOH/EtOH (9:1) at X-band frequency; see Figure 3 and Table 3 for the experimental and simulated spectra and the spin Hamiltonian parameters, obtained by simulation of the experimental spectra with the X-Sophe software package.[49] The relatively large values of A_z >200 × 10^{-4} cm^{-1}, in combination with the relative small values of $g_z \leq$ 2.18, indicate a strong in-plane ligand field with relatively small interactions to axial ligands, specifically for the H_2L^B- and H_2L^E-based systems, and this is in agreement with the structural data and solution electronic spectroscopic parameters. The small variation of A_x/g_x vs A_y/g_y values indicate a small but significant deviation from tetragonal symmetry.

Redox Properties. The electrochemical properties of the Cu^{II} complexes H_2L^B, H_2L^E, and H_2L^P were studied in H_2O, MeOH, MeCN, and DMF to investigate the stabilization of the Cu^{II} complexes and also a potential stabilization of Cu^{III} species. The experiments were performed in a three electrode glass cell under argon atmosphere, using a glassy carbon working electrode, a platinum wire as counter electrode, and an Ag/AgCl or an $Ag/AgNO_3$ reference electrode under aqueous or nonaqueous conditions, respectively. In water as solvent, 3 M NaCl was used as supporting electrolyte, and the potentials were normalized against $K_3[Fe(CN)_6]$ (E = 298 mV); in MeOH and DMF, 0.1 M Bu_4NBF_4, and in MeCN, 0.1 M Bu_4NPF_6 were used as supporting electrolytes, and the potentials were normalized against ferrocene, with −94 mV (DMF), 120 mV (MeOH), and −87 mV (MeCN). The results of the electrochemical measurements are given in Table 4.

The reversible potentials in MeCN, MeOH, H_2O, and DMF can be assigned to $Cu^{III/II}$ couples, and the corresponding redox potentials (see Table 4) are in the expected range.[26] While the cavity size of the three macrocycles studied here increases in the order $L^B < L^E < L^P$, the energy needed to oxidize the Cu^{II} complexes increases in the order $L^E < L^B < L^P$, i.e., L^E best stabilizes high-valent copper ions. The $Cu^{II/I}$ potentials could only be measured in DMF, which offers the largest electrochemical window and showed a potential at < −2 V, indicating a very high stabilization of the Cu^{II} complexes. The L^P and L^B systems have very similar $Cu^{II/I}$ potentials (slightly higher for the L^P-based couple), and the ethylene-bridged macrocycle has the most positive potential.

Radiochemistry. The three macrocycles were evaluated as potential ligands for radiolabeling with $^{64}Cu^{II}$. The radiolabeling was monitored by radio-TLC, using neutral alumina plates and 2 M NH_4OAc/MeOH (1:1) as mobile phase. $[^{64}Cu]CuCl_2$ remains at the starting position, and the complexes move with R_f values of 0.75−0.79. Standard labeling experiments, using MES/NaOH (pH 5.5) at ambient temperature, gave, as expected, no evidence for $^{64}Cu^{II}$-labeled macrocyclic bispidine ligands. Increasing the temperature to 50 °C and using a slightly higher pH significantly increased the labeling efficiency. The radiolabeling yields for H_2L^B, H_2L^E, and H_2L^P (100 μg ligand/0.1 mL aqueous buffer) as a function of time are

dx.doi.org/10.1021/ic500476u | Inorg. Chem. 2014, 53, 6698−6707

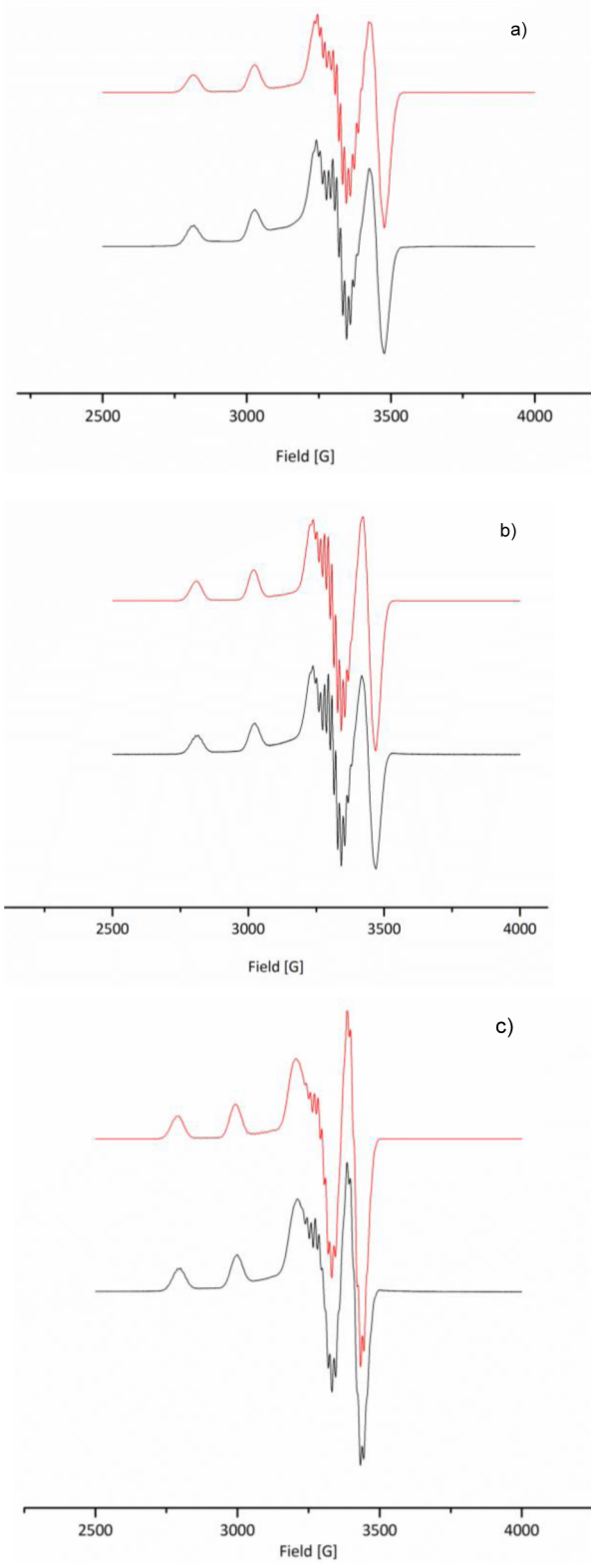

Figure 3. X-band EPR spectra (experimental, black, bottom; simulated, red, top) of the complexes (a) $[Cu(L^B)(solv)]$ at 106 K and 9.441338 GHz, (b) $[Cu(L^E)(OH_2)]$ at 107 K and 9.438382 GHz, and (c) $[Cu(L^P)(OH_2)]$ at 109 K and 9.448705 GHz.

summarized in Table 5 and show that more than 95% of the bispidine-based macrocycles are labeled with $^{64}Cu^{II}$ after 1 h. Almost quantitative labeling of the macrocyclic bispidine ligands was also achieved at lower concentrations (5 μg ligand/0.1 mL aqueous buffer) after 90 min at 50 °C. The specific activity obtained is 26 GBq/μmol for $[^{64}Cu(L^B)(solv)]$; for the other two complexes, $[^{64}Cu(L^E)(OH_2)]$ and $[^{64}Cu(L^P)(OH_2)]$, about 22 GBq/μmol was determined.

Stability Assays. The stability of the $^{64}Cu^{II}$-labeled macrocyclic bispidine-amide ligands was studied in the presence of a 3-fold excess of human superoxide dismutase (SOD) and human serum, as described before.[50] Figure 4 summarizes the quantitative results of dissociated $^{64}Cu^{II}$ in the presence of SOD and human serum protein. The complex with the benzyl-ring-based macrocycle $[^{64}Cu(L^B)(solv)]$ shows the highest stability toward SOD (transchelation of (1.5 ± 0.5) %) and serum (2.3 ± 0.9) % after 1 h of incubation at 37 °C. The radiocopper(II) dissociation from $[^{64}Cu(L^E)(OH_2)]$ and $[^{64}Cu(L^P)(OH_2)]$ is somewhat higher in the presence of excess SOD and human serum (see Supporting Information for more details). That is, the variation of the macrocycle ring size and preorganization of the macrocyclic bispidine-amide ligands strongly influence the stability of the copper(II) complexes. Obviously, the donor set and overall charge of the ligand as well as the efficiency of the shielding of the Cu^{II} center are also of importance, and this is shown with the other $^{64}Cu^{II}$ complexes subjected to the same assays (see Figure 4 and Chart 1 for ligand structures; see Supporting Information for more detail): increased shielding of the Cu^{II} center and increased electron density at the pyridine nitrogen donors of open-chain bispidine ligands lead to an increase of the complex stability,[34,37,51] and the same trend was observed in an assay using an 80-fold excess of cyclam as competing ligand.[35,51] The three complexes ^{64}Cu-L^2, ^{64}Cu-L^3, and ^{64}Cu-L^B have similar and high *in vitro* stabilities with less than 5% of $^{64}Cu^{II}$ dissociation in the SOD and human serum assays. Importantly, these assays indicate that the stability of $[^{64}Cu(L^B)(solv)]$ toward transchelation to proteins and enzymes is very similar to that of the open-chained bispidine complexes (see above) and well-established $^{64}Cu^{II}$ complexes with other ligand systems; for example, the ^{64}Cu-diamsar, ^{64}Cu-cyclam, and ^{64}Cu-NOTA complexes have SOD and human serum values of 0.6/1.7, 1.0/2.2, and 1.4/2.1.[50]

Lipophilicity. The log *P* values can be derived from the distribution of neutral compounds in a two-phase octanol–water system. For ionic compounds such as transition metal complexes, the log *D* value at physiologically relevant pH is more appropriate to predict the type of tissue in which the substance will accumulate and which clearance path it will take.[52] As expected, the Cu^{II} complexes of dioxo-tetraaza-macrocyclic bispidine ligands with aliphatic bridges, H_2L^P and H_2L^E, are more hydrophilic (log $D_{7.4}$ = −2.22 and −2.33; see Table 6) than the Cu^{II} complex of H_2L^B, which, due to the aromatic ring, is slightly lipophilic (log $D_{7.4}$ = 0.21). As a consequence of the slightly hydrophobic character, it is expected that $[^{64}Cu(L^B)(solv)]$ will be partially excreted via the hepatobiliary route. The *in vitro* stability of $[^{64}Cu(L^B)(solv)]$ in the presence of human serum and SOD is high and comparable to that of the $^{64}Cu^{II}$ complexes of the hexadentate bis-amine-tetrakis-pyridine bispidine L^2[33] and the pentadentate ligand with *p*-methoxy substitution of the pyridinyl groups L^3 (*vide supra*).[35] The log $D_{7.4}$ values of the latter radiotracers are significantly lower (^{64}Cu-L^2, −2.77; ^{64}Cu-L^3, −2.44), and therefore, there are now highly stable $^{64}Cu^{II}$ bispidine complexes with very different hydrophilicities available. This will allow one to influence the biodistribution of the biofunctionalized radiotracers by choosing the most appropriate bifunctional bispidine chelator.

dx.doi.org/10.1021/ic500476u | Inorg. Chem. 2014, 53, 6698–6707

Table 3. Simulated g- and A-values (10^{-4} cm^{-1}) of the Complexes $[Cu(L^B)(solv)]$, $[Cu(L^E)(OH_2)]$, and $[Cu(L^P)(OH_2)]$ (Simulations by X-Sophe[49]) and Literature-Known Cu^{II} Complexes of Dioxo-tetraaza Macrocyclic Ligands

	$[Cu(L^B)(O)]$	$[Cu(L^E)(OH_2)]$	$[Cu(L^P)(OH_2)]$	$[Cu(o\text{-}13N_4)]$[68]	$[Cu(o\text{-}14N_4)]$[68]
g_z	2.154	2.157	2.179	2.171	2.176
g_x	2.046	2.047	2.044	2.046	2.049
g_y	2.018	2.019	2.037	2.046	2.049
A_z	209.8	208.8	203.9	202.8	207.4
A_x	25.1	22.6	26.0	28.5	37.1
A_y	27.4	22.6	24.3	28.5	37.1
$A_{N,z}$	10.9	9.9	11.0		
$A_{N,x}$	11.7	12.3	13.2		
$A_{N,y}$	12.9	13.0	13.1		

Table 4. $Cu^{III/II}$ (in MeCN, H_2O, MeOH, and DMF) and $Cu^{II/I}$ Potentials (in DMF, Irreversible) of the Cu^{II} Complexes of H_2L^B, H_2L^E, and H_2L^P

	MeCN [mV][a]	H_2O [mV][b]	MeOH [mV][a]	DMF [mV][b]
$[Cu(L^B)(solv)]$	310	219	−17	−29; −2264 (irrev.)
$[Cu(L^E)(OH_2)]$	121	71	−88	118; −2116 (irrev.)
$[Cu(L^P)(OH_2)]$	451	418	266	−258; −2253 (irrev.)

[a]vs Fc/Fc^+. [b]vs $K_3[Fe(CN)_6]$).

Table 5. Radiochemical Yield (RCY) as a Function of Time for the ^{64}Cu-Labeling of H_2L^B, H_2L^E, and H_2L^P at 50 °C[a]

	duration [min]	RCY [%]
$[^{64}Cu(L^B)(solv)]$	5	78 (2)
	30	93 (2)
	60	>95
$[^{64}Cu(L^E)(OH_2)]$	5	83 (2)
	30	96 (2)
	60	>98
$[^{64}Cu(L^P)(OH_2)]$	5	80 (4)
	30	94 (2)
	60	>98

[a]100 μg ligand/100 μL MES-NaOH buffer at pH 6.5. Shown are the averages of two independent experiments with standard deviation in parentheses.

Biodistribution. The biodistribution data of $[^{64}Cu(L^B)(solv)]$ in rats demonstrate at 5 min post injection (p.i.) predominant activity accumulation in kidneys, liver, and intestine. In this early distribution phase, more than half of the injected dose (61 ± 7) % ID is already eliminated via the hepatobiliary system into the intestine (intestine plus feces). At this time point, the white adipose tissue (WAT), muscle, and skin also show a significant accumulation of activity. This biodistribution pattern in the early distribution phase is expected from the modest hydrophobicity of the complex. Subsequently, $[^{64}Cu(L^B)(solv)]$ is efficiently eliminated from blood and tissues (% ID/g for most organs and tissues <0.13 at 60 min p.i. and <0.07 at 24 h p.i., respectively; see Supporting Information for details) with only substantial but minor residual activity in both the kidneys (0.39 ± 0.02) % ID/g and the liver (0.42 ± 0.04) % ID/g at 60 min p.i. and only in the kidneys (0.16 ± 0.02) % ID/g after 24 h. The hepatobiliary pathway nearly exclusively contributes to the fast clearance of radioactivity observed with (80 ± 6) % ID found in the intestine at 60 min p.i. (also accounting for activity in the excretion pathway). At 24 h p.i., nearly the entire activity is found in feces and urine. The overall fast clearance from the liver and other organs and tissues indicates a high stability of the $^{64}Cu^{II}$ complex of H_2L^B, and this is in full agreement with the stability assays reported above.

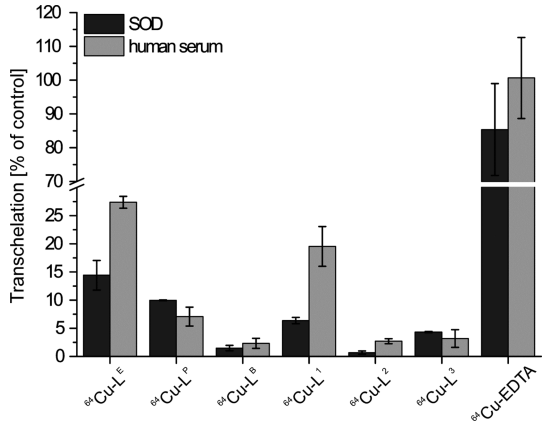

Figure 4. ^{64}Cu transchelation [% of control] in SOD (black) and human serum (gray) for ^{64}Cu-labeled H_2L^E, H_2L^P, H_2L^B, L^1, L^2, L^3, and EDTA, determined after incubation of the complexes for 1 h at 37 °C; each point represents the mean and standard deviation of three samples.

CONCLUSIONS

The ligands H_2L^B, H_2L^E, and H_2L^P are a new class of macrocyclic bispidine ligands with variable macrocycle hole shape and size and different degrees of preorganization. Because of deprotonation of the amide functions upon coordination, the Cu^{II} complexes are uncharged. Cyclic voltammetry reveals a high stability of the Cu^{II} species and also shows that Cu^{III} complexes are stabilized. The (frozen) solution EPR and electronic spectra of the Cu^{II} compounds indicate that the complexes are square-pyramidal in solution with strong in-plane ligand fields and weak interactions to axial ligands, and this is in agreement with the solid state structural data. Radiotracer experiments with $^{64}Cu^{II}$ show a relatively rapid labeling within 1 h at 50 °C with >95% yield and specific activities of 26 GBq/μmol. Challenge experiments with SOD and human serum indicate a high stability of the slightly lipophilic complex $[^{64}Cu(L^B)(solv)]$. Biodistribution studies showing rapid blood and tissue clearance support the high complex stability *in vivo*. In terms of labeling, specific activity, and stability, $[^{64}Cu(L^B)(solv)]$ is well suited for PET application, and preliminary experiments indicate that efficient biofunctionalization of H_2L^B with targeting peptides or

dx.doi.org/10.1021/ic500476u | Inorg. Chem. 2014, 53, 6698−6707

Table 6. Experimental Octanol–Water Partition Coefficients (log $D_{o/w}$) of the ^{64}Cu Bispidine-dioxo-tetraaza Macrocyclic Ligand Complexes at Different pH Values[a]

	pH 7.2	pH 7.4	pH 7.6
$[^{64}Cu(L^B)(solv)]$	0.21 (0.01)	0.21 (0.01)	0.22 (0.02)
$[^{64}Cu(L^E)(O_2H)]$	−2.35 (0.03)	−2.33 (0.03)	−2.27 (0.02)
$[^{64}Cu(L^P)(O_2H)]$	−2.22 (0.01)	−2.22 (0.01)	−2.15 (0.01)

[a]Shown are the averages of three independent experiments with the standard deviation in parentheses.

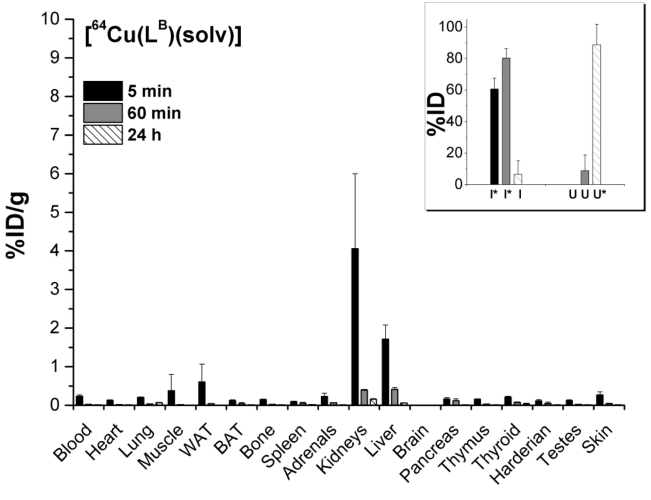

Figure 5. ^{64}Cu biodistribution of $[^{64}Cu(L^B)(solv)]$ in male Kyoto-Wistar rats, four animals per time point (mean ± SD). Insert: I*, intestine plus feces; I, intestine; U, urine; and U*, urine plus feces.

antibodies is possible by introducing a carboxylic acid linker at the aromatic bridge.

EXPERIMENTAL SECTION

General Procedures and Spectroscopic Measurements. All reactions were carried out under air. Chemicals and solvents were purchased from Sigma-Aldrich Chemie GmbH (Taufkirchen, Germany), ABCR GmbH & Co. KG (Karlsruhe, Germany), or Merck KGaA (Darmstadt, Germany) and were used without further purification. The bispidine building block (1,5-dimethyl-3,7-diazabicyclo[3.3.1]nonane) was synthesized as published.[42]

Electrochemistry was performed on a CH Instruments CHI660D electrochemical workstation, equipped with a CH Instruments Picoamp Booster. All electrochemical measurements were performed in a glass cell, covered with a Teflon cap, situated in a Faraday cage. All complex solution were prepared in degassed solvents saturated with Ar. The supporting electrolyte for nonaqueous solutions [dimethylformamide (DMF) and methanol (MeOH)] was 0.1 M tetra-*n*-butylammonium tetrafluoroborate, and for acetonitrile (MeCN), 0.1 M tetra-*n*-butylammonium hexafluorophosphate was used. All spectra in nonaqueous media were recorded with an $Ag/AgNO_3$ reference electrode, a glassy carbon working electrode, and a platinum wire as counter electrode. Aqueous solutions contained 3 M sodium chloride (NaCl) as supporting electrolyte and were performed with an Ag/AgCl reference electrode, a glassy carbon working electrode and a platinum wire as counter electrode. Electrochemical measurements in nonaqueous media were normalized versus ferrocene, where ferrocene had the following potentials: DMF (−94 mV), MeOH (120 mV), and MeCN (−87 mV); in aqueous media, potentials were normalized against potassium hexacyano ferrate ($K_3[Fe(CN)_6]$) with 298 mV. Potentials marked with a * are assigned as irreversible.

UV–vis-NIR spectra were recorded with a Jasco V-570 UV–vis-near-IR spectrometer as methanolic solutions. NMR spectra were recorded on a Bruker Avance I (200 MHz), and chemical shifts of ^{1}H and ^{13}C are referenced to solvent resonances ($CDCl_3$).

EPR measurements were performed on a Bruker ELEXSYS-E-500 instrument with liquid nitrogen, in frozen methanol/ethanol (9:1) solution. The spin Hamiltonian parameters were obtained by simulation of the experimental data with the XSophe software package.[53,54] ESI-MS spectra were recorded on a Bruker ApexQe hybrid 9.4 T FT-ICR.

Elemental analyses were obtained from a CHN-O-vario EL by the "Mikroanalytische Labor", Department of Organic Chemistry, University of Heidelberg.

Crystal structural data and deteremination details are given as Supporting Information. Data collection was performed with a Bruker AXS Smart 1000 CCD diffractometer (Mo–K_α radiation, sealed tube, graphite monochromator) or with an Agilent Technologies Supernova-E CCD diffractometer (Mo– or Cu–K_α radiation, microfocus tube multilayer mirror optics). Correction for air and detector absorption were performed, as well as Lorentz and polarization effects.[55,56] Semiempirical multiscan methods[56–59] were used to correct the absorption by the crystal or an analytical[56,60] or numerical treatment.[56,60,61] Using Olex2,[62] structures were solved by charge flipping[63,64] or conventional direct methods.[65,66] Structures were refined by full-matrix least-squares methods based on F^2 against unique reflections.[65,66] All non-hydrogen atoms were given anisotropic displacement parameters and were put at calculated positions and refined with a riding model. CCDC 988221-988226 contains the supplementary crystallographic data for this Article. These data can be obtained free of charge from The Cambridge Crystallographic Data Centre via www.ccdc.cam.ac.uk/data_request/cif.

Radiochemistry. The production of ^{64}Cu was performed at a PET cyclotron as described in detail elsewhere.[67] The yields of the nuclear reaction $^{64}Ni(p,n)^{64}Cu$ were between 3.6–5.2 GBq (EOB) with specific activities of 150–250 GBq/μmol Cu. The bispidine ligands were radiolabeled by adding 50–200 MBq of $[^{64}Cu]CuCl_2$ to 0.1 to 100 μg of H_2L^B, H_2L^E, and H_2L^P dissolved in 100 μL of 0.05 M 2-[*N*-morpholino]ethansulfonic acid (MES)-NaOH buffer (pH 5.5, 6.0, and 6.5). The radiolabeling yield was determined by radio-TLC (stationary phase, neutral alumina plates (Merck, F254); mobile phase, methanol/2 M ammonium acetate (1/1, v/v); $^{64}CuCl_2$, R_f = 0; and ^{64}Cu–bispidine complexes, R_f = 0.75–0.79). Radio-TLC chromatograms were scanned using a radioisotope thin layer analyzer (Rita Star, raytest). The labeling efficiency was investigated as a function of pH, time, temperature, and ligand concentration. For biodistribution experiments, H_2L^B (10 μg dissolved in 250 μL of 1 M MES/NaOH buffer (pH 6.5)) was radiolabeled with $[^{64}Cu]CuCl_2$ (120 MBq) for 90 min at 50 °C. Radio-TLC confirmed full complexation. The radiochemical purity of $[^{64}Cu(L^B)(solv)]$ was also determined by radio-HPLC on a HPLC Hewlett-Packard System (Series 1100); activity detector, Raytest Ramona Star; column, Zorbax (Agilent) 300SB-C18, 300 Å, 5 μm, 250 mm × 9.4 mm; gradient, eluent A (water + 0.1% TFA) and eluent B (acetonitrile + 0.1% TFA), 5 min 95% A, 10 min 95% A to 95% B, 10 min 95% B, and 1 mL/min ($[^{64}Cu(L^B)(solv)]$; t_R = 13.6 min).

Determination of the Distribution Ratio log $D_{o/w}$ at 25 ± 1 °C. Information about the lipophilicity of the $^{64}Cu^{II}$-labeled bispidine dioxotetraaza macrocycles H_2L^B, H_2L^E, and H_2L^P was obtained by distribution experiments in buffer/1-octanol mixtures. Aqueous solutions of the bispidine ligands (1 mM in MES/NaOH, pH 6.5) were pre-equilibrated in the presence of 100 μM $Cu(NO_3)_2$, spiked with $[^{64}Cu]CuCl_2$ (3 MBq) for 1 h at 50 °C. Full complexation was checked by radio-TLC to give no evidence of free $^{64}Cu^{II}$. Then, 50 μL of the $^{64}Cu^{II}$-labeled bispidine complexes, dissolved in MES/NaOH

dx.doi.org/10.1021/ic500476u | Inorg. Chem. 2014, 53, 6698–6707

buffer, was taken and added to 450 μL of 0.05 M 4-(2-hydroxyethyl)-1-piperazine ethanesulfonic acid (HEPES)-NaOH solutions (pH 7.2, 7.4, and 7.6). The aqueous buffered solutions (HEPES/NaOH buffer) consist of 100 μM bispidine ligands, 10 μM $Cu(NO_3)_2$, and 300 kBq $[^{64}Cu]CuCl_2$. The distribution experiments in 1-octanol/buffer systems were performed at 25 ± 1 °C in microcentrifuge tubes (2 cm^3) by means of mechanical shaking for 30 min. The phase ratio $V_{(1\text{-octanol})}/V_{(aq)}$ was 1:1 (0.5 cm^3 each). All samples were centrifuged and the phases separated, and the copper(II) concentration was determined in both phases radiometrically using γ-radiation [^{64}Cu, NaI(Tl) scintillation counter automatic gamma counter 1480, Wizard 3″, PerkinElmer]. The results are the average values of three independent experiments.

***In Vitro* Stability Studies in the Presence of Human Serum and SOD.** The detailed procedure of the *in vitro* assays in SOD and human serum was published previously.[50] The radiolabeling conditions of the ligands H_2L^E, H_2L^P, and H_2L^B are described above. The other bispidine derivatives (L^1, L^2, and L^3) were radiolabeled as follows: to each ligand (10 nmol, stock solution of 1 mg/mL diluted in H_2O), was added $[^{64}Cu]CuCl_2$ (10−14 MBq in 100 μL of 0.1 M MES/NaOH-buffer, pH 5.5) followed by 20 min of incubation at 25 °C. Formation of the complexes was verified by radio-TLC, using methanol/2 M ammonium acetate (pH 6) (1/1, v/v) on a neutral alumina plate ($^{64}CuCl_2$, R_f = 0; ^{64}Cu-bispidine complexes, R_f = 0.75−0.79). The radiochemical yield was higher than 99%; otherwise, they were rejected. For SOD experiments, ^{64}Cu-labeled ligands (0.1 nmol, 1.5 μL) or $[^{64}Cu]CuCl_2$ as reference were added to SOD (0.3 nmol, 10 μg). The mixtures were incubated for 1 h at 37 °C followed by adding 1 volume of native sample buffer. The samples were separated using nonreducing and nondenaturing polyacrylamide gel electrophoresis (PAGE), and after electrophoresis, the gel was exposed for 10 min to an imaging plate (Fujifilm). Following electronic autoradiography using a radioluminography laser scanner, the gel was stained with PageBlue protein staining solution (Thermo Fisher Scientific) according to the manufacturer's instructions. Quantitative analysis of average band intensities was performed with the Advanced Image Data Analysis (AIDA) program (Raytest). For serum experiments, aliquots of human serum "off the clot" (Biochrom AG) were filtered using syringe filters with a pore size of 0.45 μm. After mixing filtered serum (220 μL) with 1 M HEPES/NaOH buffer at pH 7.4 (45 μL), [^{64}Cu]Cu-labeled ligands were added. Following incubation for 1 h at 37 °C, 2× Laemmli sample buffer (400 μL, Bio-Rad Laboratories) was added. Importantly, the Laemmli buffer was not supplemented with any reducing agent, and the samples were not heated. The mixtures were separated using nonreducing SDS−polyacrylamide gel electrophoresis (SDS−PAGE). After electrophoresis and exposure of the gel to an imaging plate (Fujifilm) for 10 min, electronic autoradiography was accomplished using a radioluminography laser scanner. Finally, the gel was stained with PageBlue protein staining solution (Thermo Fisher Scientific) according to the manufacturer's instructions. As for the SOD challenge, quantitative analyses of average band intensities were performed with the AIDA software.

Biodistribution Experiments. All animal experiments were carried out in male Wistar rats (Wistar-Kyoto strain; aged 7−8 weeks, 140−195 g; Harlan Winkelmann GmbH, Borchen, Germany) according to the guidelines of the German Regulations for Animal Welfare. The protocol was approved by the local Ethical Committee for Animal Experiments. The biodistribution experiments were performed as published in detail elsewhere.[35,51] The injection volume of $[^{64}Cu(L^B)(solv)]$ (0.4−2.6 MBq; radiochemical purity, >99% after HPLC separation; specific activity, 12 MBq/μg $[^{64}Cu(L^B)(solv)]$; dissolved in electrolyte solution E-153 (Serumwerk Bernburg, Germany) at pH 7.2) was 0.5 mL. The ^{64}Cu activity concentration in organs and tissues was calculated as either the percentage of the injected dose per gram tissue (% ID/g tissue) or, for both intestine and urine, the percentage of the injected dose (% ID).

Syntheses. *N*,*N*′-Bis(chloroacetyl)-1,2-phenylenediamine, *N*,*N*′-bis(chloroacetyl)-1,2-ethylenediamine, and *N*,*N*′-bis(chloroacetyl)-1,3-propylenediamine were prepared as described in the literature.[43,28]

2,10-Dioxo-6,19-dimethyl-1,4,8,11-tetraazatetracyclo-[12.3.3.16,19.012,17]-heneicosa-12,14,16-triene (H_2L^B). 1,5-Dimethyl-diazabicyclo[3.3.1]nonane (0.77 g; 5.00 mmol; 1 equiv) and *N*,*N*′-bis(chloroacetyl)-1,2-phenylendiamine (1.30 g; 5.00 mmol; 1 equiv) were refluxed with Na_2CO_3 (5.30 g; 50.00 mmol; 10 equiv) in acetonitrile (250.00 mL) for 24 h. After cooling to room temperature, the solid was removed by filtration, and the solvent was evaporated. The residue was redissolved in a small amount of ethanol, and after the addition of water, the solution was left to crystallize uncovered at room temperature. The product (1.11 g; 3.24 mmol; 65% yield) forms colorless block shaped crystals that were dried *in vaccuo*. ^{1}H NMR ($CDCl_3$, 200 MHz): δ [ppm] = 0.80 (s, C**H**$_3$, 6H), 1.16 (s, C**H**$_2$, 2H), 2.14−2.19 (d, C**H**$_{2,ax,eq}$, *J* = 10.7 Hz, 4H), 2.76−2.82 (d, C**H**$_{2,ax,eq}$, *J* = 11.0 Hz, 4H), 2.97 (s, NC**H**$_2$C═O, 4H), 7.06−7.11 (m, **H**$_{arom}$, 2H), 7.93−7.98 (m, **H**$_{arom}$, 2H), 9.49 (bs, N**H**, 2H). ^{13}C NMR ($CDCl_3$, 100 MHz): δ [ppm] = 25.77, 33.10, 46.18, 62.56, 63.90, 121.30, 124.80, 127.81, 169.20. Elemental analysis: calcd C(66.65), H(7.65), N(16.36); exp C(66.73), H(7.65), N(16.36). Mass spectrometry: HR-ESI MS (MeOH) *m*/*z* = 343.21299 (calcd 343.21340) $[H_2L^B+H]^+$, 365.19490 (calcd 365.19535) $[H_2L^B+Na]^+$, 381.16887 (calcd 381.16928) $[H_2L^B+K]^+$, 707.40063 (calcd 707.40092) $[2\ H_2L^B+Na]^+$, 1049.60673 (1049.60650) $[3\ H_2L^B+Na]^+$.

2,10-Dioxo-6,15-dimethyl-1,4,8,11-tetraazatricyclo-[8.3.3.16,15]heptadecane (H_2L^E). 1,5-Dimethyldiaza-bicyclo[3.3.1]-nonane (0.77 g; 5.00 mmol; 1 equiv) and *N*,*N*′-bis(chloroacetyl)-1,2-ethylendiamine (1.06 g; 5.00 mmol; 1 equiv) were refluxed with Na_2CO_3 (5.30 g; 50.00 mmol; 10 equiv) in acetonitrile (250.00 mL) for 24 h. After cooling to room temperature, the solid was removed by filtration, and the solvent was evaporated. The product (0.50 g; 1.70 mmol; 34% yield) was crystallized as small white crystals from hot water. ^{1}H NMR ($CDCl_3$, 200 MHz): δ [ppm] = 0.77 (s, C**H**$_3$, 6H), 1.09 (s, C**H**$_2$, 2H),1.87−1.94 (d, C**H**$_{2,ax,eq}$, *J* = 11.3 Hz, 2H), 1.98 (s, NC**H**$_2$C═O, 2H), 2.29−2.36 (d, C**H**$_{2ax,eq}$, *J* = 10.8 Hz, 2H), 2.49−2.55 (d, C**H**$_{2,ax,eq}$, *J* = 10.8 Hz, 2H), 2.79−2.85 (d, C**H**$_{2ax,eq}$, *J* = 11.3 Hz, 2H), 2.89 (s, NC**H**$_2$C═O, 2H), 3.20−3.22 (m, NHC**H**$_2$, 2H),3.39−3.45 (m, C**H**$_2$NH, 2H). ^{13}C NMR ($CDCl_3$, 100 MHz): δ [ppm] = 25.46, 32.88, 37.53, 41.39, 42.79, 46.10, 58.76, 60.59, 62.54, 65.05, 171.33, 174.11. Elemental analysis: calcd (H_2L^E +1 H_2O) calcd C(57.65), H(9.03), N(17.93); obsd C(57.54), H(9.17), N(17.75). Mass spectrometry: HR-ESI MS (MeOH) *m*/*z* = 295.21298 (calcd 295.21340) $[H_2L^E+H]^+$, 611.40053 (calcd 611.40092) $[2\ H_2L^E+Na]^+$, 905.60640 (calcd 905.60650) $[3\ H_2L^E+Na]^+$.

2,10-Dioxo-6,16-dimethyl-1,4,-8,11-tetraazatricyclo-[9.3.3.16,16]oxtadecane (H_2L^P). 1,5-Dimethyldiaza-bicyclo[3.3.1]-nonane (0.77 g; 5.00 mmol; 1 equiv) and *N*,*N*′-bis(chloroacetyl)-1,3-propylendiamine (1.13 g; 5.00 mmol; 1 equiv) were refluxed with Na_2CO_3 (5.30 g; 50.00 mmol; 10 equiv) in acetonitrile (250.00 mL) for 24 h. After cooling to room temperature, the solid was removed by filtration, and the solvent was evaporated. The product (1.14 g; 3.71 mmol; 74% yield) was crystallized as small colorless needles from aqueous ethanol by evaporation at room temperature. ^{1}H NMR ($CDCl_3$, 200 MHz): δ [ppm] = 0.78 (s, C**H**$_3$, 6H), 1.09 (s, C**H**$_2$, 2H), 1.70−1.78 (quint, *J* = 5.56, $CH_2C\mathbf{H}_2CH_2$, 2H), 1.96−2.02 (d, *J* = 10.7 Hz, C**H**$_{2ax,eq}$, 4H), 2.67−2.73 (d, *J* = 10.9 Hz, C**H**$_{2ax,eq}$, 4H), 2.82 (s, NC**H**$_2$C═O, 4H), 3.37−3.45 (q, *J* = 5.18 Hz, C**H**$_2$, 4H). ^{13}C NMR ($CDCl_3$, 100 MHz): δ [ppm] = 25.08, 28.57, 32.89, 39.72, 46.53, 62.36, 64.58, 170.96. Elemental analysis: (H_2L^P+1 H_2O) calcd C(58.87), H(9.26), N(17.16); exp C(58.89), H(9.26), N(17.10). Mass spectrometry (HR-ESI MS (MeOH)): *m*/*z* = 309.22859 (calcd 309.22905) $[H_2L^P+H]^+$, 331.21054 (calcd 311.21100) $[H_2L^P+Na]^+$, 347.18449 (calcd 347.18493) $[H_2L^P+K]^+$, 617.44981 (calcd 617.45028) $[2\ H_2L^P+H]^+$.

[$Cu^{II}(L^B)$(O)]. The ligand H_2L^B (50 mg; 146.01 μmol; 1 equiv) was dissolved in MeOH (1 mL) and a solution of $Cu(OAc)_2 \times 2\ H_2O$ (29.2 mg; 146.01 μmol) in MeOH (1 mL) was added while stirring. After stirring at room temperature overnight, the purple precipitate was separated by filtration, redissolved in MeOH, and subjected to ether diffusion. The analytically pure complex crystallized as long red-purple needles (33 mg, 81.68 μmol, 56% yield). Elemental analysis: ($[Cu^{II}(L^B)]$+1 H_2O) calcd C(55.09), H(6.47), N(12.85); expd

dx.doi.org/10.1021/ic500476u | *Inorg. Chem.* 2014, 53, 6698−6707

C(54.96), H(6.29), N(13.02). UV−vis spectroscopy: λ = 483 nm (20704 cm^{-1}), ε = 149 M^{-1} cm^{-1}; cyclic voltammetry 310 mV (MeCN), −17 mV (MeOH), −29 mV, −2264 mV* (DMF), 219 mV (H_2O).

[$Cu^{II}(L^E)(OH_2)$]. The ligand H_2L^E (50 mg; 169.84 μmol; 1 equiv) was dissolved in MeOH (1 mL) and a solution of $Cu(OAc)_2 \times 2H_2O$ (34.0 mg; 169.84 μmol) in MeOH (1 mL) was added while stirring. After stirring at room temperature overnight, the purple precipitate was separated by filtration, redissolved in MeOH, and subjected to ether diffusion. The analytically pure complex crystallized as long red purple needles (33 mg, 81.68 μmol, 56% yield). Elemental analysis: ([$Cu^{II}(L^E)$]+1.5 MeOH) calcd C(49.06), H(7.48), N(13.87); exp C(49.10), H(7.56), N(14.05). UV−vis spectroscopy: λ = 476 nm (21008 cm^{-1}), ε = 189 M^{-1} cm^{-1}; cyclic voltammetry 121 mV (MeCN), −88 mV (MeOH), 118 mV, −2116 mV* (DMF), 71 mV (H_2O).

[$Cu^{II}(L^P)(OH_2)$]. The ligand H_2L^P (50 mg; 162.12 μmol; 1 equiv) was dissolved in MeOH (1 mL), and a solution of $Cu(OAc)_2 \times 2\ H_2O$ (32.0 mg; 162.12 μmol) in MeOH (1 mL) was added while stirring. After stirring at room temperature overnight, the purple solution was evaporated to dryness and the residue redissolved in MeOH and subjected to ether diffusion. The analytically pure complex crystallized as long red purple needles (33 mg, 81.68 μmol, 56% yield). Suitable crystals were obtained by slow evaporation of a methanolic solution. Elemental analysis: ([$Cu^{II}(L^P)$]+2 H_2O) calcd C(47.34), H(7.45), N(13.80); exp C(47.32), H(7.16), N(13.80). UV−vis spectroscopy: λ = 524 nm (19084 cm^{-1}), ε = 117 M^{-1} cm^{-1}; cyclic voltammetry 451 mV (MeCN), 266 mV (MeOH), −254 mV, −2253 mV* (DMF), 418 mV (H_2O).

■ ASSOCIATED CONTENT

Ⓢ Supporting Information

Details of the crystallographic experiments, a plot of the crystal structure of [$Cu^{II}(L^B)(O)$], spectra of the metal-free ligands, UV−vis spectra and CV's of the complexes reported, and details of the SOD and human serum assays and the biodistribution experiments. This material is available free of charge via the Internet at http://pubs.acs.org. CCDC 988221-988226 contains the supplementary crystallographic data which can be obtained free of charge from The Cambridge Crystallographic Data Centre via www.ccdc.cam.ac.uk/data_request/cif.

■ AUTHOR INFORMATION

Corresponding Authors

*(P.C.) Fax: +49-6221-546617. E-mail: peter.comba@aci.uni-heidelberg.de.

*(H.S.) Fax: +49-351-2603232. E-mail: h.stephan@hzdr.de.

Notes

The authors declare no competing financial interest.

■ ACKNOWLEDGMENTS

Financial support by the German Science Foundation (DFG), the University of Heidelberg, and the Helmholtz Association (funding through the Helmholtz Virtual Institute Nano-Tracking, Agreement Number VH-VI-421, and the Helmholtz-Portfolio Topic "Technologie und Medizin − Multimodale Bildgebung zur Aufklärung des In-vivo-Verhaltens von polymeren Biomaterialien") are gratefully acknowledged. We are grateful to Professor H. Wadepohl for the collection of the X-ray data and helpful discussions, and to Madlen Matterna, Janine Partsch, and Regina Herrlich for technical assistance.

■ DEDICATION

Dedicated to Professor Bernd Johannsen on the occasion of his 75th birthday.

■ REFERENCES

(1) Shokeen, M.; Anderson, C. J. *Acc. Chem. Res.* **2009**, *42*, 832−841.
(2) Blower, P. J.; Lewis, J. S.; Zweit, J. *Nucl. Med. Biol.* **1996**, *23*, 957−980.
(3) Schmidt-Ott, W.-D. *Z. Phys.* **1959**, *154*, 286−293.
(4) Cooper, M. S.; Ma, M. T.; Sunassee, K.; Shaw, K. P.; Williams, J.; Paul, R. L.; Donnelly, P. S.; Blower, P. J. *Bioconjugate Chem.* **2012**, *23*, 1029.
(5) Cutler, C. S.; Hennkens, H. M.; Sisay, N.; Huclier-Markai, S.; Jurisson, S. S. *Chem. Rev.* **2013**, *113*, 858−883.
(6) Holland, J. P.; Barnard, P. J.; Collision, D.; Dilworth, J. R.; Edge, R.; Green, J. C.; Heslop, J. M.; McInnes, E. J. L.; Salzmann, C. G.; Thompson, A. L. *Eur. J. Inorg. Chem.* **2008**, *22*, 3549.
(7) Bu, H. X.; Zhand, Z. H.; An, D. L.; Chen, Y. T.; Shinoya, M.; Kimura, E. *Inorg. Chem.* **1996**, *241* (1), 125.
(8) Martell, A. E.; Motekaitis, R. J.; Clarke, E. T.; Delgado, R.; Sun, Y.; Ma, R. *Supramol. Chem.* **1996**, *20* (3−4), 353.
(9) Chaves, S.; Delgado, R.; Frausto da Silva, J. J. R. *Talanta* **1992**, *39* (3), 249.
(10) Delgado, R.; Frausto da Silva, J. J. R. *Talanta* **1982**, *29* (10), 815.
(11) Woodin, K. S.; Heroux, K. J.; Boswell, C. A.; Wong, E. H.; Weisman, G. R.; Niu, W.; Tomellini, S. A.; Anerson, C. J.; Zakharov, L. N.; Reingold, A. L. *Inorg. Chem.* **2005**, 4829.
(12) Wong, E. H.; Weisman, G. R.; Hill, D. C.; Reed, D. P.; Rogers, M. E.; Condon, J. S.; Fagan, M. A.; Calabrese, J. C.; Lam, K.-C.; Guzei, I. A.; Rheingold, A. L. *J. Am. Chem. Soc.* **2000**, *122*, 10561−10572.
(13) Boswell, C. A.; Sun, X.; Niu, W. J.; Weisman, G. R.; Wong, E. H.; Rheingold, A. L.; Anderson, C. J. *J. Med. Chem.* **2004**, *47*, 1465−1474.
(14) Geue, R. J.; Hambley, T. W.; Harrowfield, J. M.; Sargeson, A. M.; Snow, M. R. *J. Am. Chem. Soc.* **1984**, *106*, 5478−5488.
(15) Sargeson, A. M. *Coord. Chem. Rev.* **1996**, *151*, 89−114.
(16) Di Bartolo, N. M.; Sargeson, A. M.; Donlevy, T. M.; Smith, S. V. *J. Chem. Soc., Dalton Trans.* **2001**, 2303−2309.
(17) Cabbiness, D. K.; Margerum, D. W. *J. Am. Chem. Soc.* **1969**, *61*, 6540−6541.
(18) Cabbiness, D.; Margerum, D. W. *J. Am. Chem. Soc.* **1970**, *92*, 2152−2153.
(19) Jones-Wilson, T. M.; Deal, K. A.; Anderson, C. J.; McCarthy, D. W.; Kovacs, Z.; Motekaitis, R. J.; Sherry, A. D.; Martell, A. E.; Welch, M. J. *Nucl. Med. Biol.* **1998**, *25*, 523−530.
(20) Bass, L. A.; Wang, M.; Welch, M. J.; Anderson, C. J. *Bioconjugate Chem.* **2000**, *11*, 527−532.
(21) Odendaal, A. Y.; Fiamengo, A. L.; Ferdani, R.; Wadas, T. J.; Hill, D. C.; Peng, Y.; Heroux, K. J.; Golen, J. A.; Rheingold, A. L.; Anderson, C. J.; Weisman, G. R.; Wong, E. H. *Inorg. Chem.* **2011**, *50*, 3078−3086.
(22) Lattuada, L.; Barge, A.; Cravotto, G.; Giovenzana, G. B.; Tei, L. *Chem. Soc. Rev.* **2011**, *40*, 3019−3049.
(23) Denat, F.; Brandès, S.; Guilard, R. *Synlett* **2000**, *5*, 561−574.
(24) Chong, H.-S.; Song, H. A.; Kang, C. S.; Le, T.; Sun, X.; Dadwal, M.; Lee, H.; Lan, X.; Chen, Y.; Dai, A. *Chem. Commun.* **2011**, *47*, 5584−5586.
(25) Lewis, E. A.; Allan, C. C.; Boyle, R. W.; Archibald, S. J. *Tetrahedron Lett.* **2004**, *45*, 3059−3062.
(26) Kimura, E. *J. Coord. Chem.* **1986**, *15*, 1−28.
(27) Sharma, S. K.; Hundal, G.; Gupta, R. *Eur. J. Inorg. Chem.* **2010**, 621−636.
(28) Antunes, P.; Delgado, R.; Drew, M. G. B.; Felix, V.; Maecke, H. *Inorg. Chem.* **2007**, *46* (8), 3144−3153.
(29) Barnard, P. J.; Holland, J. P.; Bayly, S. R.; Wadas, T. J.; Anderson, C. J. *Inorg. Chem.* **2009**, *48*, 7117−7126.

(30) Vin Tan, K.; Pellegrini, P. A.; Skelton, B. W.; Hogan, C. F.; Greguric, I.; Barnard, P. J. *Inorg. Chem.* **2014**, *53*, 468−477.
(31) Comba, P.; Nuber, B.; Ramlow, A. *J. Chem. Soc., Dalton Trans.* **1997**, 347−352.
(32) Comba, P.; Kerscher, M.; Schiek, W. *Prog. Inorg. Chem.* **2007**, *55*, 613−704.
(33) Juran, S.; Walther, M.; Stephan, H.; Bergmann, R.; Steinbach, J.; Kraus, W.; Emmerling, F.; Comba, P. *Bioconjugate Chem.* **2009**, *20*, 347−359.
(34) Comba, P.; Morgen, M.; Wadepohl, H. *Inorg. Chem.* **2013**, *52*, 6481−6501.
(35) Comba, P.; Hunoldt, S.; Morgen, M.; Pietzsch, J.; Stephan, H.; Wadepohl, H. *Inorg. Chem.* **2013**, *52*, 8131−8143.
(36) Mannich, C.; Mohs, P. *Chem. Ber.* **1930**, *B63*, 608−612.
(37) Comba, P.; Kerscher, M. *Coord. Chem. Rev.* **2009**, *253*, 564−574.
(38) Comba, P. Oxidation Catalysis with High-Valent Nonheme Iron Complexes, in *Molecular Catalysis*; Gade, L. H., Hofmann, P., Eds.; Wiley-VCH: Weinheim, Germany, 2014.
(39) Comba, P.; Pritzkow, H.; Schiek, W. *Angew. Chem.* **2001**, *113*, 2556.
(40) Islam, M. J. l.; Miller, E. J.; Gordner, J. S.; Patel, D.; Wang, Z. *Tetrahedron Lett.* **2013**, 2133−2136.
(41) Comba, P.; Daumann, L.; Lefebvre, J.; Linti, G.; Martin, B.; Straub, J.; Zessin, T. *Aust. J. Chem.* **2009**, *62*, 1238−1245.
(42) Kuznetsov, A. I.; Basargin, E. B.; Ba, M. K.; Moskovin, A. S.; Miroshnichenko, I. V.; Bosnikov, M. Y. *Chem. Heterocycl. Compd.* **1989**, 647.
(43) Bradshaw, J. S.; Krakowiak, K. E.; An, A.; Izatt, R. M. J. *Heterocyclic Chem.* **1990**, *27*, 2113−2116.
(44) Comba, P.; Okon, N.; Remenyi, R. *J. Comput. Chem.* **1999**, *20*, 781−785.
(45) Comba, P.; Fath, A.; Kühner, A.; Nuber, B. *J. Chem. Soc., Dalton Trans.* **1997**, 1889−1898.
(46) Comba, P. *Coord. Chem. Rev.* **1999**, *182*, 343−371.
(47) Comba, P.; Schiek, W. *Coord. Chem. Rev.* **2003**, *238*−*239*, 21−29.
(48) Comba, P.; Hambley, T. W.; Hitchman, M. A.; Stratemeier, H. *Inorg. Chem.* **1995**, *34*, 3903−3911.
(49) Hanson, G. R.; Gates, K. E.; Noble, C. J.; Griffin, M.; Mitchell, A.; Benson, S. *J. Inorg. Biochem.* **2004**, *98*, 903−916.
(50) Zarschler, K.; Kubeil, M.; Stephan, H. *RSC Adv.* **2014**, *4*, 10157−10164.
(51) Comba, P.; Emmerling, F.; Jakob, M.; Kraus, W.; Kubeil, M.; Morgen, M.; Pietzsch, J.; Stephan, H. *Dalton Trans.* **2013**, *42*, 6142−6148.
(52) Comba, P.; Martin, B.; Sanyal, A.; Stephan, H. *Dalton Trans.* **2013**, *42*, 11066−11073.
(53) Wang, D.; Hanson, G. R. *J. Magn. Reson. A* **1995**, *117*, 1−8.
(54) Wang, D.; Hanson, G. R. *Appl. Magn. Reson.* **1996**, *11*, 401−415.
(55) *Bruker SAINT Bruker AXS*; Bruker: Madison, WI, 1997−2008.
(56) *SCALE3 ABSPACK CrysAlisPro*; Agilent Technologies UK Ltd., Oxford, U.K., 2011−2013.
(57) Blessing, R. H. *Acta Crystallogr., Sect. A* **1995**, *51*, 33−38.
(58) Sheldrick, G. M. *SADABS-2004-2008*, SADABS-2004/1; Bruker AXS: Karlsruhe, Germany, 2004−2008.
(59) Sheldrick, G. M. *TWINABS*; Bruker AXS: Karlsruhe, Germany, 2004−2008.
(60) Clark, R. C.; Reid, J. S. *Acta Crystallogr., Sect. A* **1995**, *51*, 887−897.
(61) Sheldrick, G. M. *SADABS*; Bruker AXS: Karlsruhe, Germany, 2004−2012.
(62) Dolomanov, O. V.; Bourhis, L. J.; Gildea, R. J.; Howard, J. A. K.; Puschmann, H. *J. Appl. Crystallogr.* **2009**, *42*, 339−341.
(63) Palatinus, L.; Chapuis, G. *J. Appl. Crystallogr.* **2007**, *40*, 786−790.
(64) Palatinus, L. *SUPERFLIP*; EPF Lausanne: Switzerland, 2007.
(65) Sheldrick, G. M. *SHELXS-97*; University Göttingen: Göttingen, Germany, 1997.
(66) Sheldrick, G. M. *Acta Crystallogr., Sect. A* **2008**, *64*, 112−122.
(67) Thieme, S.; Walther, M.; Pietzsch, H.-J.; Henniger, J.; Preusche, S.; Maeding, P.; Steinbach, J. *Appl. Radiat. Isot.* **2012**, *70*, 602−608.
(68) Miyoshi, K.; Tanaka, H.; Kimura, E.; Tsuboyama, S.; Murata, S.; Shimizu, H.; Ishizu, K. *Inorg. Chim. Acta* **1983**, *78*, 23.